Progress In Electromagnetics Research B, Vol. 28, 163–182, 2011

ROOM TEMPERATURE TERAHERTZ PHOTODETECTION IN ATOMIC AND QUANTUM WELL REALIZED STRUCTURES

M. Zyaei †

Department of Electrical Engineering
Islamic Azad University, Ajabshir Branch, Ajabshir, Iran

A. Rostami

School of Emerging Engineering Technologies
University of Tabriz, Tabriz, Iran

H. Haji Khanmohamadi

Department of Electrical Engineering
Islamic Azad University, Ajabshir Branch, Ajabshir, Iran

H. Rasooli Saghai

School of Emerging Engineering Technologies
University of Tabriz, Tabriz, Iran

Abstract—A novel kind of room temperature terahertz photodetector based on Electromagnetically Induced Transparency (EIT) is presented. The main idea for room temperature and THz range operation is reduction of dark current which is done by converting of the incoming terahertz signal (long-wavelength Infrared signal) to short-wavelength field through EIT phenomena. For realization of this idea, we examine EIT phenomena in multi levels atomic system and quantum wells cascade structures. In the proposed structure the quantum interference between long wavelength and short-wavelength radiation modifies the absorption characteristic of short-wavelength probe field. By this means, the terahertz signal does not interact directly with ground state electrons, but affects on the absorption characteristics of

Received 15 December 2010, Accepted 1 February 2011, Scheduled 7 February 2011
Corresponding author: Majed Zyaei (M_zyaei_sh@yahoo.com).
† Also with Departments of Computer Engineering, Islamic Azad University, Ajabshir Branch, Ajabshir, Iran.

the short-wavelength or visible probe optical field which directly interact with ground state electrons. Therefore, the important thermionic dark current in terahertz detection, can be strongly reduced. So, the proposed idea is appropriate for terahertz and room temperature applications.

1. INTRODUCTION

Nowadays infrared photodetectors and their applications are in the focus of much attention, especially in terahertz and room temperature applications [1–3]. Terahertz ($1 \sim 10\,\mathrm{THZ}$) or far-infrared ($30 \sim 300\,\mu\mathrm{m}$) photodetectors could be useful in military, security, medical imaging, astronomy, wireless communication and gas sensing. However the dark current noise which determines the signal-noise ratio is important [4, 5]. The dark current noise inhibits the correct detection of these low level (terahertz) signals and also this is more critical in room temperatures. The main challenge is reduction of the dark current noise in photodetectors [6, 7]. One of the important parts of dark current is thermionic emission, simply thermal excitation of the carriers to higher energy levels and this is not related to the radiation that is got from the target. In the terahertz ($30 \sim 300\,\mu\mathrm{m}$ or $1 \sim 10\,\mathrm{THz}$) photodetectors, the incoming photon energy is ($4 \sim 41\,\mathrm{meV}$) and maybe in the order of electron thermal broadening ($\mathrm{KT} \sim 6\,\mathrm{meV}$–$25\,\mathrm{meV}$ for $77\,\mathrm{K}$–$300\,\mathrm{K}$), so in conventional infrared photodetectors, the incoming photon or the environment temperature directly excites the ground state electrons to higher energy levels and in the presence of electric field, these electrons are collected as a photocurrent and thermionic dark current [4–7]. Therefore in room temperature and terahertz applications, the dark current inhibits the correct detection of signal, so we have electron transport problems in this range of detection [4, 6, 7]. However in our proposed EIT-based photodetector, which use the nonlinear characteristic of light, the electromagnetic field of terahertz light interfere with the electromagnetic field of short-wavelength ($1 \sim 2\,\mu\mathrm{m}$) probe field and modify the light absorption characteristic of probe field. Therefore the incoming terahertz IR light and the environment temperature do not directly excite ground state electrons. In fact we translate the incoming terahertz-IR signal to short-wavelength optical field through EIT Phenomena [8, 9], where such problems are not critical in this range of detection. Researchers in the proposed schema in reference [10, 11] depicted that with EIT phenomena can defeat the mentioned problems, but the electron extract and electron transport problems were still the major problems in terahertz photodetectors and were not discussed and designed

before. In this paper a new structure for the electron transport problem will be introduced by the quantum well cascade structure. Therefore, a complete terahertz quantum well photodetector structure based on EIT can be achieved. For room temperature application we study the effect of environment temperature on the EIT based photodetector operation. Our main purpose is to reduce the effect of environment temperature on photodetector. Furthermore, in this paper for the reduction of unfavorable effect of temperature on terahertz photodetector an optimized 6-level quantum well realized structure will be analyzed and simulated. The organization of this paper is as follow:

In Section 2, the mathematical background for calculation of the susceptibility in different atomic systems and quantum well structures and the effect of environment temperature will be presented. Simulation results and discussion will be illustrated in Section 3. Finally, the paper is going to end with a short conclusion.

2. MATHEMATICAL BACKGROUND

This section shows basic mathematical calculation for EIT based terahertz infrared photodetector. Fig. 1 shows a 4-levels atomic system. The probe field, control field and Infrared field are applied between states 1-4, 2-4 and 3-2 respectively. In the interaction picture and under rotating-wave approximation we can write the total Hamiltonian as [8, 9]:

$$H = \hbar \begin{bmatrix} \nu_1 & 0 & 0 & -\Omega_p e^{i\nu_p t} \\ 0 & \nu_2 & -\Omega_{IR} e^{i\nu_{IR} t} & -\Omega_c e^{i\nu_c t} \\ 0 & -\Omega_{IR} e^{-i\nu_{IR} t} & \nu_3 & 0 \\ -\Omega_p e^{-i\nu_p t} & -\Omega_c e^{-i\nu_c t} & 0 & \nu_4 \end{bmatrix} \quad (1)$$

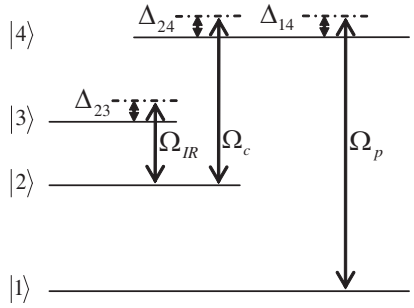

Figure 1. Schematic of 4 -Levels atomic system.

Using the density matrix formalism, under the electro-dipole and rotating-wave approximations, we begin to describe the dynamic response of the proposed 4-levels atomic structure as [12, 13]:

$$\dot{\rho}_{ij} = -\frac{i}{\hbar}\sum\left(H_{i\,k}\,\rho_{k\,j} - \rho_{i\,k}\,H_{k\,j}\right) - \frac{1}{2}\sum\left(\Gamma_{i\,k}\,\rho_{k\,j} + \rho_{i\,k}\Gamma_{k\,i}\right) \quad (2)$$

$$\dot{\rho}_{21} = -[i(\Delta_p - \Delta_c) + \gamma_{21}]\rho_{21} + i\Omega_{IR}\rho_{31} + i\Omega_c\rho_{41} - i\Omega_p\rho_{24} \quad (3)$$

$$\dot{\rho}_{31} = -[i(\Delta_p + \Delta_{IR} - \Delta_c) + \gamma_{31}]\rho_{31} + i\Omega_{IR}\rho_{21} - i\Omega_p\rho_{34} \quad (4)$$

$$\dot{\rho}_{41} = -[i\Delta_p + \gamma_{41}]\rho_{41} + i\Omega_p\rho_{11} + i\Omega_c\rho_{21} - i\Omega_p\rho_{44} \quad (5)$$

where $\Delta_p = \nu_{41} - \nu_p$, $\Delta_c = \nu_{42} - \nu_c$ and $\Delta_{IR} = \nu_{32} - \nu_{IR}$ are probe detuning, control detuning and IR signals detuning form their respective atomic transition. We have assumed that the Rabi frequencies of the probe (Ω_p), control (Ω_c) and IR signal (Ω_{IR}) are real. In the steady state we have obtained the analytical solution for the above equations.

$$\rho_{41} = \frac{\left[\gamma_{21} + i(\Delta_p - \Delta_c) + \frac{\Omega_{IR}^2}{\alpha}\right]\,\Omega_p}{\left[\Omega_c^2 + [i\Delta_p + \gamma_{41}]\,[i(\Delta_p - \Delta_c) + \gamma_{21}] + \frac{\Omega_{IR}^2(i\Delta_p + \gamma_{41})}{\alpha}\right]} \quad (6)$$

where $\alpha = [i(\Delta_p - \Delta_c + \Delta_{IR}) + \gamma_{31}]$. In the weak field limit on the probe, the complex susceptibility at the probe field frequency is obtained from optical polarization.

$$P = \varepsilon_0 E_p[\chi(\omega_p)\; e^{-i\omega_p t} + c.c] \quad (7)$$

$$P = 2\,N\wp[\rho_{41}e^{-i\omega_p t} + c.c] \quad (8)$$

where N is the density of atom and $\wp$ is dipole moment matrix element of transition. The probe absorption is proportional to the imaginary part of ρ_{41}. The real and imagery part of susceptibility $\chi = \chi' + i\chi''$ lead to dispersion and absorption respectively. The intensity absorption and dispersion coefficient are given by $\alpha = \omega_p n_0 \chi''/c$ and $\beta = \omega_p n_0 \chi'/2c$ respectively. The behavior of 4-level atomic system can be clearly determined by evaluation of zeros and poles of ρ_{41}.

$$poles(\rho_{41}) = \begin{bmatrix} \nu_p \overset{\Delta}{\cong} \nu_{41} + \sqrt{(\Omega_c^2 + \Omega_{IR}^2)} \\ \nu_p \overset{\Delta}{\cong} \nu_{41} - \sqrt{(\Omega_c^2 + \Omega_{IR}^2)} \\ \nu_p \overset{\Delta}{\cong} \nu_{41} \end{bmatrix} \quad (9)$$

$$zeros(\rho_{41}) = \begin{bmatrix} \nu_p \overset{\Delta}{\cong} (\nu_{41} + \Omega_{IR}) \\ \nu_p \overset{\Delta}{\cong} (\nu_{41} - \Omega_{IR}) \end{bmatrix}$$

For simplicity in the above equations, we suppose $\Delta_c = \Delta_{IR} = 0$ and $\gamma_{ij} = 0$. However for given γ, when the fields are detuned the zeros and poles locations changes and the response of the system is completely different. But there is an interesting case when $\Delta_c = \Delta_{IR}$ the zeros and poles locations are independent from detuning and will be fix (it is explained in the next section).

Atomic systems can be realized with the multi quantum well structures. In many aspects the eigen-states in quantum well are like atomic systems [12, 14]. In the atomic systems if two fields are coupled and interfere with each other and one of them is strong, so the optical stark effect is created. There is a shift in absorption characteristic, so we see two new absorptions where there was transparency. In this case we say the atomic states are splitting and this is known as an Electromagnetic Induced Transparency (EIT). In quantum well structures the stark effect can be created with the coupling of two wells and the EIT like condition may be appeared [15–18]. The barrier potential between two well is thin (coupled wells) and the eigen-states are in the same energy or in the range of electron — LO phonon scattering [4, 5, 7] or electron–electron scattering and other scattering processes, so the wave functions of two wells can see each other through thin barrier (resonant-mode). Thus the two new states $|a\rangle, |c\rangle$ are created. This effect is like to stark effect in an atomic system which is introduced by strong pump field. Fig. 2 shows the schematic of asymmetric double barrier quantum well structure as an EIT based photodetector cell. In this structure the probe filed and terahertz infrared filed are applied respectively.

In the interaction picture, the total Hamiltonian for this 4-

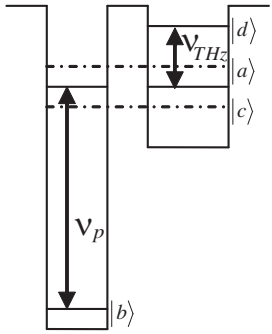

Figure 2. Asymmetric double barrier quantum well structure as an EIT based Terahertz (Long wave length infrared) photodetector cell.

subband quantum well structure can be written as [17–19]:

$$H=\hbar\begin{pmatrix} \nu_b & 0 & -\Omega_p e^{i\nu_p t} & -q\Omega_p e^{i\nu_p t} \\ 0 & \nu_d & -\Omega_{THz} e^{i\nu_{THz} t} & -k\Omega_{THz} e^{i\nu_{ITHz} t} \\ -\Omega_p e^{-i\nu_p t} & -\Omega_{THz} e^{-i\nu_{ITHz} t} & \nu_c & 0 \\ -q\Omega_p e^{-i\nu_p t} & -k\Omega_{THz} e^{-i\nu_{THz} t} & 0 & \nu_a \end{pmatrix} \tag{10}$$

The Rabi frequencies of the probe signal (Ω_P) and THz-signal (Ω_{THz}) have been assumed to be real. Using the density matrix formalism, one may describe the dynamic response of the proposed 4-subband quantum well structure. Under the electro-dipole and rotating-wave approximations (this method has been utilized to describe the results in experimental [13–15] and also theoretical works [17–19]), the time-dependent density-matrix equations of motion can be obtained as [12]:

$$\dot{\rho}_{ab} = -\left[i\left(\Delta_p + \frac{\omega_S}{2}\right) + \Gamma_{ab}\right]\rho_{ab} + iq\Omega_p\rho_{bb} - iq\Omega_p\rho_{aa} + ik\Omega_{THz}\rho_{db} - i\Omega_p\rho_{ac} \tag{11}$$

$$\dot{\rho}_{cb} = -\left[i\left(\Delta_p - \frac{\omega_S}{2}\right) + \Gamma_{cb}\right]\rho_{cb} + i\Omega_p\rho_{bb} + i\Omega_{THz}\rho_{db} - iq\Omega_p\rho_{ca} - i\Omega_p\rho_{cc} \tag{12}$$

$$\dot{\rho}_{dc} = -\left[i\left(\Delta_{THz} + \frac{\omega_S}{2}\right) + \Gamma_{dc}\right]\rho_{dc} - i\Omega_p\rho_{db} - i\Omega_{THz}\rho_{dd} + i\Omega_{THz}\rho_{cc} + ik\Omega_{THz}\rho_{ac} \tag{13}$$

$$\dot{\rho}_{db} = -i(\Delta_p + \Delta_{THz} + \Gamma_{db})\rho_{db} + i\Omega_{THz}\rho_{cb} + ik\Omega_{THz}\rho_{ab} - i\Omega_p\rho_{dc} - iq\Omega_p\rho_{da} \tag{14}$$

$$\dot{\rho}_{da} = -\left[i\left(\Delta_{THz} - \frac{\omega_S}{2}\right) + \Gamma_{da}\right]\rho_{da} - iq\Omega_p\rho_{db} - ik\Omega_{THz}\rho_{dd} + ik\Omega_{THz}\rho_{aa} + i\Omega_{THz}\rho_{ca} \tag{15}$$

$$\dot{\rho}_{ac} = -[i\omega_S + \Gamma_{ac}]\rho_{ac} - i\Omega_p\rho_{ab} + iq\Omega_p\rho_{bc} - i\Omega_{THz}\rho_{ad} + ik\Omega_{THz}\rho_{dc} \tag{16}$$

where $\omega_s = \nu_{ab} - \nu_{cb}$, $\nu_0 = \frac{\nu_{ab}+\nu_{cb}}{2}$, $\nu_0' = \frac{\nu_{ad}+\nu_{cd}}{2}$ and $\Delta_p = \nu_0 - \upsilon_p$, $\Delta_{THz} = \nu_0' - \upsilon_{THz}$. Also in the carrier conservation condition we have:

$$\rho_{bb} + \rho_{dd} + \rho_{cc} + \rho_{aa} = 1 \tag{17}$$

The population and dephasing decay rates are added phenomenologically in the above density matrix equations. The population decay rate for subband $|j\rangle$ (due to LO-phonon emission events) is denoted by γ_j. The total decay rates are given by:

$\Gamma_{cb} = \gamma_c + \gamma_{cb}^{dph}$, $\Gamma_{ab} = \gamma_a + \gamma_{ab}^{dph}$, $\Gamma_{db} = \gamma_d + \gamma_{db}^{dph}$ ($\gamma_d = \gamma_{cd} + \gamma_{ad}$),
$\Gamma_{ac} = \gamma_a + \gamma_c + \gamma_{ac}^{dph}$, $\Gamma_{cd} = \gamma_c + \gamma_d + \gamma_{cd}^{dph}$ and $\Gamma_{ad} = \gamma_a + \gamma_d + \gamma_{ad}^{dph}$.

In these expressions γ_{ij} (determined by electron-electron, interfaces roughness, and phonon scattering process) is the dephasing decay rate

of the $|i\rangle \leftrightarrow |j\rangle$ transition. In this case the probe field interacts with both the sub band transitions $|b\rangle \leftrightarrow |c\rangle$ and $|b\rangle \leftrightarrow |a\rangle$ simultaneously with the Rabi frequencies Ω_p and $q\Omega_p$ ($q = {}^{\mu_{ab}}/_{\mu_{cb}}$ is dipole moment of relevant transition). On the other hand the terahertz-infrared field interacts with both $|d\rangle \leftrightarrow |c\rangle$ and $|d\rangle \leftrightarrow |a\rangle$ with the Rabi frequencies Ω_{THz} and $K\Omega_p$ (where $K = {}^{\mu_{ad}}/_{\mu_{cd}}$ is dipole moment of relevant transition).

Similar to pervious calculations, we obtain susceptibility as:

$$\chi_p^{(1)} = \frac{2N/\varepsilon_0\hbar[\wp_{ab}^2(L_1L_2+\Omega_{THz}^2)+\wp_{cb}^2(-K\Omega_{THz}\Omega_{THz}+qL_3L_2+qK\Omega_{THz}^2)]}{L_1L_2L_3 + L_3\Omega_{THz}^2 + L_1 + K^2\Omega_{THz}^2} \tag{18}$$

where $L_1 = [i(\Delta_p - \frac{\omega_s}{2}) + \Gamma_{cb}]$, $L_2 = [i(\Delta_p + \Delta_{IR}) + \Gamma_{db}]$, $L_3 = [i(\Delta_p + \frac{\omega_s}{2}) + \Gamma_{ab}]$, $K = \frac{\mu_{da}}{\mu_{dc}}$, $q = \frac{\mu_{ab}}{\mu_{cb}}$.

The exact behavior of system is shown from the poles and zeros location.

$$\begin{aligned} poles(\chi_p) &= \begin{bmatrix} \nu_p \overset{\Delta}{\cong} \nu_0 + \sqrt{\frac{\omega_s^2}{4} + 2\Omega_{THz}^2}) \\ \nu_p \overset{\Delta}{\cong} \nu_0 - \sqrt{\frac{\omega_s^2}{4} + 2\Omega_{THz}^2}) \\ \nu_p \overset{\Delta}{\cong} \nu_0 \end{bmatrix} \\ zeros(\chi_p) &= \begin{bmatrix} \nu_p = \nu_0 + \Omega_{THz}^2 \\ \nu_p = \nu_0 - \Omega_{THz}^2 \end{bmatrix} \end{aligned} \tag{19}$$

For simplicity, in the above equation we assumed $\Delta_{THz} = 0$, $\gamma_{ij} = 0$ and $q = K = 1$.

In Fig. 2 the electrons are not directly excited by terahertz infrared radiation because the quantum interference between the states controls the absorption characteristic. For terahertz radiation detection we should bias this structure for exciting the electrons and collecting them for getting the current. Fig. 2 does not support this because we really cannot bias the asymmetric quantum well really for exciting electrons. So in this paper the EIT-based quantum well cascade detector (QWCD) structure is introduced.

The EIT-based quantum well cascade detector (QWCD) structure is presented in Fig. 3 and the mathematical basis for proposed idea is developed.

In Fig. 3 there are two regions; the asymmetric double barrier well (Active region) and the wells between them (electron transport region). In this structure we can use the benefit of photovoltaic devices like zero bias, low dark current, high responsivity and so on.

The EIT-based QCD considered in this paper is a GaN/AlGaN heterostructure where the first quantum well of the period is n doped

in order to populate the first energy level $E1$ in the conduction band with electrons (the nominal doping concentration of $5 \times 10^{11}\,\mathrm{cm}^{-2}$ has been considered). Fig. 4 presents wave functions associated with each energy subband in one period of the device. The layer widths in one period from left to right (active region and ladder) are: 20, 16, 10, 22, 10, 30, 20, 6, 20, 6, 20, 7, 20, 8, 20, 10, 20, 11, 20, 13, 20 and 15Å respectively. The energy levels and envelope functions have been calculated using 1D Schrödinger-Poisson self-consistent equations in a single band approximation.

The active region of the QCD structure is schematically presented in Fig. 2 which consists of two coupled asymmetric quantum wells. It should be noted that the mid barrier inside the shallow well in Fig. 4 is placed to control the THz signal wavelength as a freedom degree of design.

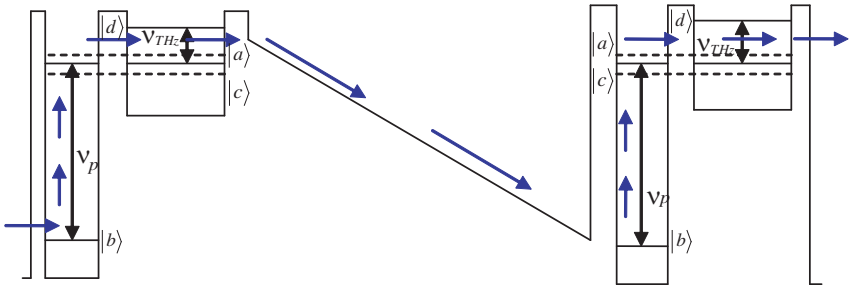

Figure 3. The EIT- based quantum well cascade detector (QWCD) structure.

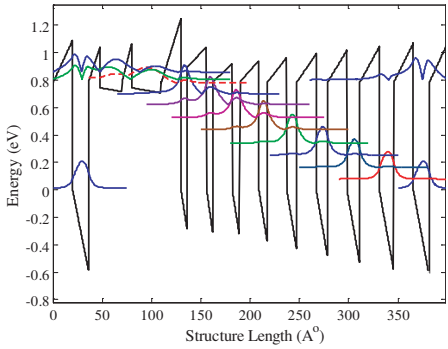

Figure 4. Schematic of the conduction band profile, wave functions and associated energy levels of the EIT- based terahertz quantum cascade photodetector.

A convenient operational definition of temperature is that, it is a measure of the average translational kinetic energy associated with the disordered microscopic motion of atoms and molecules. The molecules of matter at ordinary temperatures can be considered to be in ceaseless, random motion at high speeds. The average translational kinetic energy for these molecules can be deduced from the Boltzmann distribution. Where the Boltzmann distribution is:

$$f(E) = A\, e^{\frac{-E}{KT}} \tag{20}$$

If Boltzmann distribution is applied to the motion of a molecule in one dimension, it becomes:

$$f(v_z) = \sqrt{\frac{m}{2\pi KT}}\; e^{\frac{-mv_z^2}{2KT}} \tag{21}$$

This distribution function can be used to calculate the average value of the square of the velocity as:

$$\left\langle v_z^2 \right\rangle = \sqrt{\frac{m}{2\pi KT}} \int\limits_{-\infty}^{\infty} v_z^2\, e^{-mv_z^2/2KT}\, dv_z \tag{22}$$

$$\left\langle v_z^2 \right\rangle = \sqrt{\frac{m}{2\pi KT}}\; \frac{\sqrt{\pi}}{2} \left[\frac{2KT}{m}\right]^{3/2} = \frac{KT}{m} \tag{23}$$

The average kinetic energy for one dimension is then:

$$\frac{1}{2}\, m \left\langle v_z^2 \right\rangle = \frac{KT}{2} \tag{24}$$

And for three dimensions of such motion the average kinetic energy is:

$$\left\langle \frac{1}{2}\, m\, v^2 \right\rangle = \frac{3}{2} KT \tag{25}$$

We can with confidence just multiply the one-dimensional result by three since the different components of velocity are independent of each other. This assignment of $kT/2$ of energy to each degree of freedom of the molecule's motion is called equipartition of energy. This microscopic kinetic energy is often called thermal energy and this expression is useful in defining the kinetic temperature. Therefore the environment average thermal energy in our proposed structures is considered as follows:

$$E_{thermal} = \left\langle \frac{1}{2}\, m\, v^2 \right\rangle = \frac{3}{2} KT \tag{26}$$

where K and T is Boltzmann constant and temperature verses Kelvin, respectively. The above energy will be added to the THz-signal energy as follow:

$$E_T = E_{IR} + E_{thermal} \tag{27}$$

Finally, we introduce another atomic system and its quantum well realized structure for managing the effect of environment temperature. Fig. 5 shows the schematic of this atomic system and its quantum well realized version.

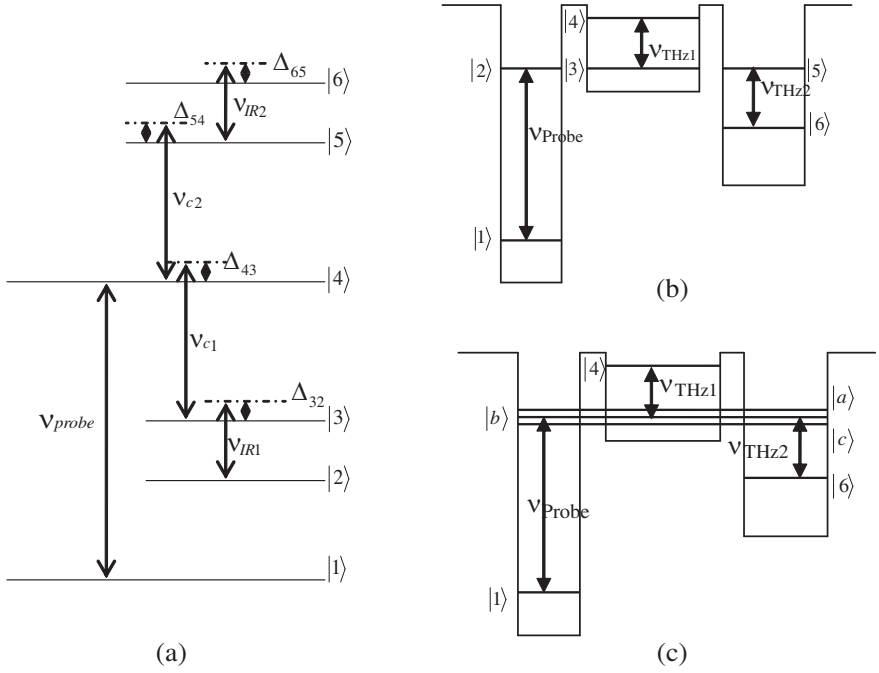

Figure 5. (a) Schematic of 6-levels atomic system, (b) uncoupled quantum well, (c) coupled quantum well structure.

Similar to previous calculations, we obtain susceptibility as:

$$\chi_{41}^{(1)} = \left[\frac{2N\wp^2/\varepsilon_0\hbar \left[-L_4L_5 + \frac{-\Omega_{IR1}^2[L_5]}{L_1} + \frac{-\Omega_{IR2}^2[L_4]}{L_2} + \frac{-\Omega_{IR1}^2\Omega_{IR2}^2}{L_1L_2} \right]}{\left[\frac{-L_3\Omega_{IR1}^2\Omega_{IR2}^2}{L_1L_2}\right] + \left[\frac{-L_3L_4\Omega_{IR2}^2}{L_2}\right] + \left[\frac{-L_3L_5\Omega_{IR1}^2}{L_1}\right] + [-L_3L_4L_5] + [-L_4\Omega_{c2}^2] + [-L_5\Omega_{c1}^2] + \left[\frac{-\Omega_{c1}^2\Omega_{IR2}^2}{L_2}\right] + \left[\frac{-\Omega_{c2}^2\Omega_{IR1}^2}{L_1}\right]} \right] \quad (28)$$

where $L_1 = [i(\Delta_p - \Delta_{c1} - \Delta_{IR1}) + \gamma_{21}]$, $L_2 = [i(\Delta_p + \Delta_{c1} + \Delta_{IR2}) + \gamma_{61}]$, $L_3 = [i\Delta_p + \gamma_{41}]$, $L_4 = [i(\Delta_p - \Delta_{c1}) + \gamma_{31}]$, $L_5 = [i(\Delta_p + \Delta_{c2}) + \gamma_{51}]$.

3. SIMULATIONS AND RESULTS

In this section simulated results of transmission coefficient for the probe field in the different proposed structures are presented and discussed. The effect of infrared and control fields on the transmission coefficient of the probe field for 4-levels atomic system (Fig. 1) is shown in Fig. 6(a). The Autler-Townes doublet is created with the definite control field and broadens with the increase of control field intensity. In the presence of IR field, a central sharp absorption peak appears and the Autler-Townes doublet make broad due to IR intensity. Fig. 6(b) shows the effect of IR intensity on the transmission coefficient spectra. It is obvious the magnitude of central absorption peak increases with IR intensity and also the width of sharp absorption peak broaden with IR intensity. If the IR field is a long-wavelengths infrared field and the probe field short wavelength or visible optical field, the absorption characteristic of the short-wavelength probe field on resonance translate the absorption characteristic of IR field. So with EIT we modify the absorption characteristic of visible probe. These features make the present system suitable for a kind of detectors.

The two different situations are shown in Fig. 7(a). In the case of zero- detuning (all three fields on resonance $\Delta_{IR} = \Delta_c = 0$), there is an absorption exactly in the center of the transmission band due to IR signal. However if we have nonzero-detuning in the IR field and this detune becomes $\Delta_{IR} \approx \Omega_c$, a new transparency peak appears near the maximum absorption of the system. Thus it is also possible to turn absorption into transparency and this is also suitable idea for a kind of

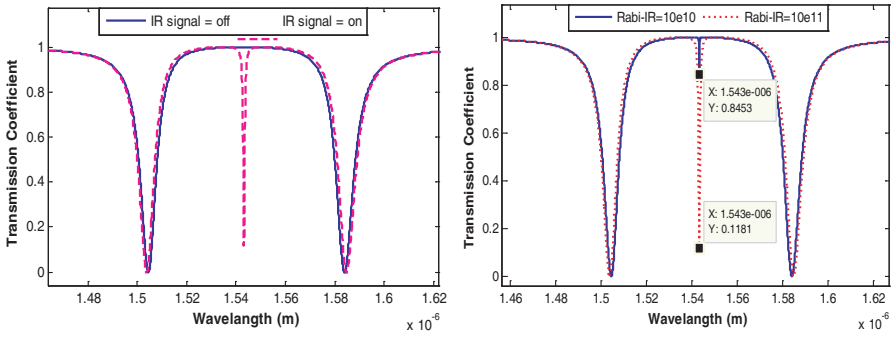

Figure 6. (a) Transmission coefficient vs. wavelength in the presence and absence of IR field. (b) Transmission coefficient of probe field vs. wavelength for different IR intensities (for 4-levels atomic system).

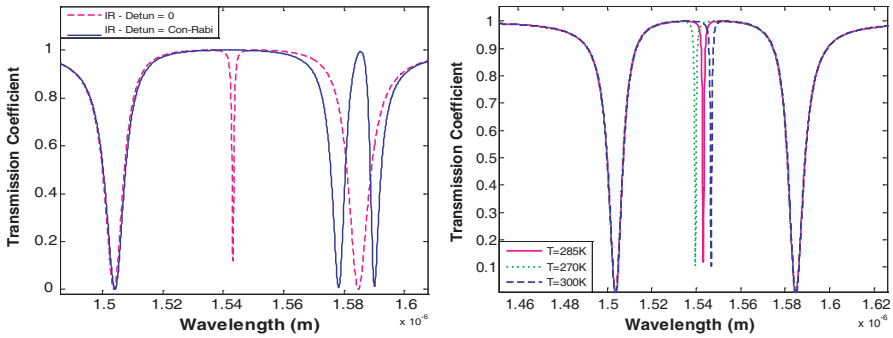

Figure 7. (a) Transmission coefficient vs. wavelength in zero-detuning and non-zero detuning. (b) Transmission coefficient vs. wavelength for different environment temperatures (for 4-levels atomic system).

detectors. The effect of the environment temperature can be considered as detuning effect. Fig. 7(b) shows the wavelength of the central absorption changes with temperature. It is observed that 7 nm shift of wavelength for 30°C of temperature changes. When refraction index of material increases ($n_{refractive} = 1 \rightarrow 3.5(GaAs)$), the wavelength temperature coefficient decreases ($\Delta\lambda/\Delta T = 0.23/°\mathrm{C} \rightarrow 66\,\mathrm{pm}/°\mathrm{C}$) that is so excellent from practical implementation point of view.

Atomic structure can be realize with multi quantum well structure, so we investigate the characteristics of realized quantum well cascade photodetector structure where the active region of this structure is proposed in Fig. 2. According to the optical susceptibility (Eq. (18)), we will see two sharp absorption (Autler-Townes-like doublet) in the system transmission coefficient which are related to the transition, $|b\rangle \leftrightarrow |a\rangle$ and $|b\rangle \leftrightarrow |c\rangle$ respectively (Fig. 8(a)). The width of this Autler-Townes-like doublet is proportional to the splitting energy ($\langle 3|\, V_0\, |4\rangle$). Solving the Schrödinger equation for this 4 — subbands quantum well shows that the splitting energy can changes in range of $10 \sim 100$ milli electron volt, and also the magnitude of dipole moment ratios (K and q) are closer to one. The effect of THz-IR radiation on the transmission coefficient of Quantum well cascade active region is shown in Fig. 8(b). In the presence of THz-IR radiation, a new sharp absorption is created in between the Autler-Townes-like doublet. The effect of THz-IR radiation intensity on the transmission coefficient is shown in Fig. 8(c). It is clear that increasing the THz-IR intensity, causes an increase in the amplitude of new peak absorption.

Another interesting case also is happen. Fig. 8(d) Shows the effect of IR radiation on the transmission coefficient, when the IR field is in

resonance with the transition energy $|d\rangle \leftrightarrow |a\rangle$ or $|d\rangle \leftrightarrow |c\rangle$ (detuning $= \pm 50\%$). We see a new sharp transparency in the spectrum where there was absorption.

The magnitude of this new transparency (detuning $= \pm 50\%$) is changed with the IR intensity (Fig. 9(a)) and this is important from photodetection point of view.

The effect of environment temperature on the transmission coefficient of realized quantum well cascade active region is shown in Fig. 9(b). The environment thermal energy may be added to the incoming target THz- IR signal and this effect inhibits the correct THz-IR detection in the conventional photodetectors. However we show that this problem is not critical in our proposed EIT based asymmetric quantum well cascade structure. In the EIT based structure the environment thermal energy cannot directly excite ground state

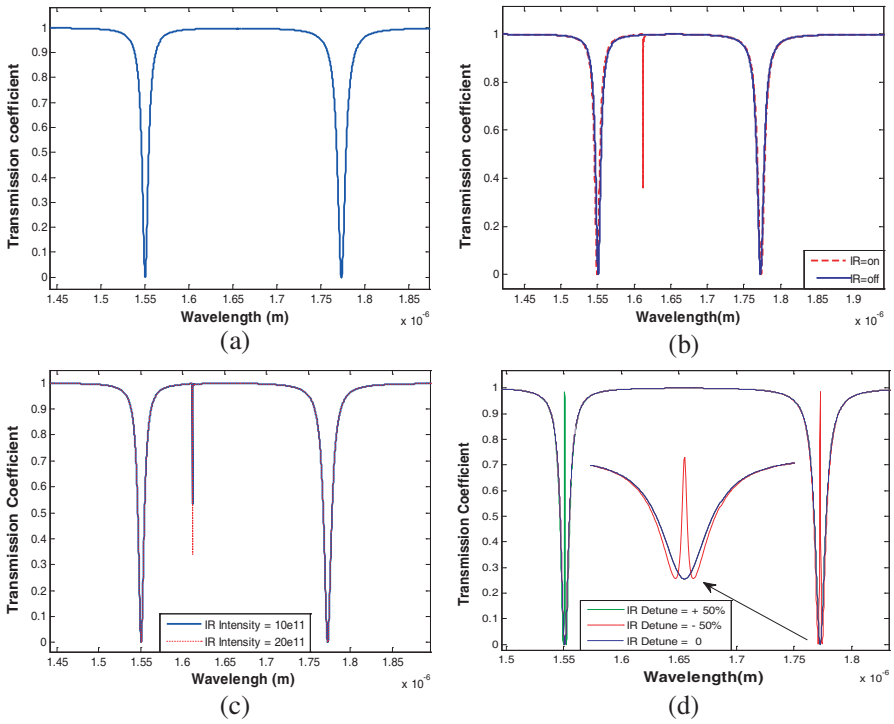

Figure 8. Transmission coefficient verses wavelength. (a) In quantum well cascade structure (Active region). (b) In the presence and absence of THz-IR field. (c) For different IR intensities (4-subband quantum well system). (d) For detuning $= \pm 50\%$ (IR transition $|d\rangle \leftrightarrow |a\rangle$ and $|d\rangle \leftrightarrow |c\rangle$).

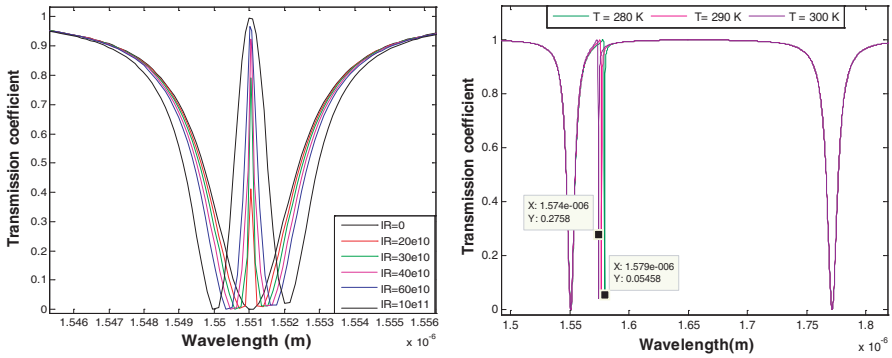

(a) (b)

Figure 9. Transmission coefficient Vs. wavelength. (a) With detuning $= \pm 50\%$ for different TH-IR intensities. (b) For different environment temperatures (4-subband quantum well system).

electrons (state $|b\rangle$ is populated but state $|d\rangle$ is not) but it causes some detuning in THz-IR field. If we couple THz-IR without detuning, the environment temperature is added to THz-IR signal and case a detuning (for $T = 0^\circ\, K \rightarrow 300^\circ\, K$, $\Delta\lambda \approx 80\,\text{nm}$). Fig. 9(b) shows 5 nm shift of wavelength for 20°C of room temperature variation. It should be mentioned that when the refraction index of material increased ($n_{refractive} = 1 \rightarrow 3.5\,(for\, GaAs)$), the wavelength temperature coefficient can be decreased ($\Delta\lambda/\Delta T = 0.2\,\text{nm}/^\circ\text{C} \rightarrow 60\,\text{pm}/^\circ\text{C}$) where that is so excellent for purposes of practical implementation.

In the above atomic system and realized quantum well as active region of cascade structure, we minimized the environment temperature effect on the operation of the systems but cannot cancel out exactly this effect. Now, we show that in proposed 6-level atomic system and the quantum well realized structure, the effect of environment temperature completely can be removed. This behavior of the new structure is very interesting from the room-temperature photodetectors point of view. Fig. 10(a) shows the effect of two control field radiations on the transmission coefficient of this atomic system. In the presence of control field Ω_{c1} Autler-Townes-like doublet is created and broadens with control field Ω_{c2}. As we expect from Fig. 10(b) in the presence of IR-signals, a sharp absorption peak is observed in center of the Autler-Townes-like doublet and its magnitude changes with IR radiation. So really THz-IR-photodetector operation is obtained.

Figure 10(c) shows the effect of different environment temperatures on the system operation. It is observed that when temperature is not zero, two other absorption peaks are appeared and with increas-

ing the temperature the observed peaks location change. But, we found that the appeared peak in the central part of the spectrum is independent of temperature and the magnitude of central peak varying with IR intensity. So this is interesting for room temperature operation.

In Figs. 5(b) and (c) the realized quantum well structure for 6-level atomic structure has been showed. Now we investigate the transmission characteristic of realized quantum well structure. Fig. 11(a) shows the transmission coefficient of probe field (short wavelength) for quantum well realized structure. Three absorption peaks are shown in the transmission coefficient of optical probe field, which are related to transitions $|1\rangle \leftrightarrow |a\rangle$, $|1\rangle \leftrightarrow |c\rangle$, $|1\rangle \leftrightarrow |b\rangle$ respectively. From the THz-IR photodetector point of view, in the transmission coefficient of probe field the two sharp absorption peak

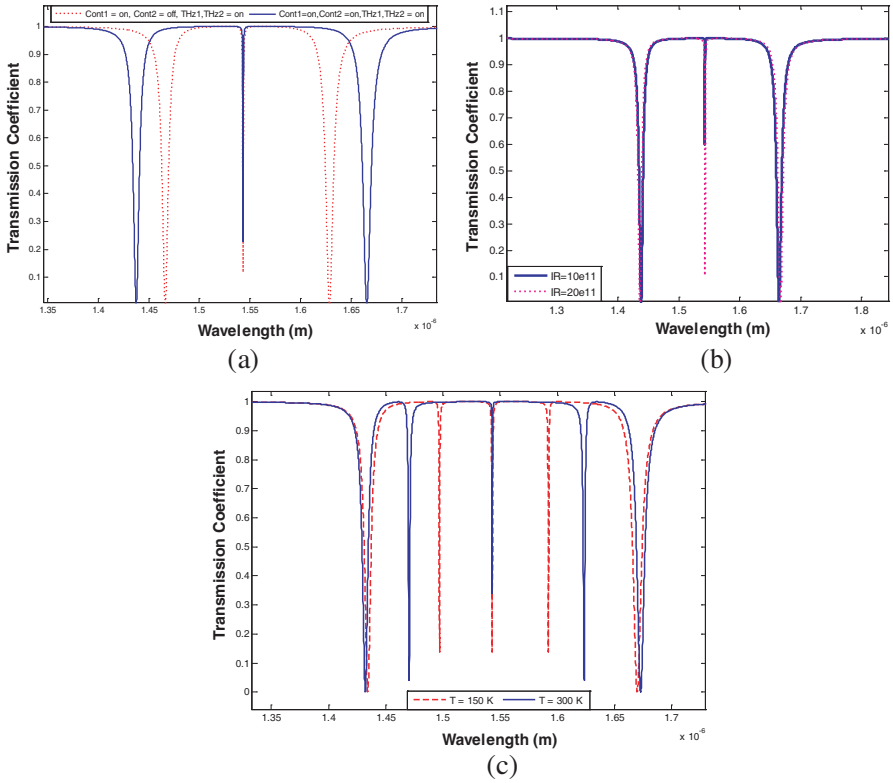

Figure 10. Transmission coefficient vs. wavelength. (a) In the presence of THz-IR fields and control fields. (b) For different THz-IR intensities. (c) For different environment temperatures (6-levels atomic system).

are appeared in the presence of THz-IR radiations. And the magnitude of these absorption peaks is proportional to the THz-IR radiation intensities (Fig. 11(b)). These two sharp absorption peaks are related to either of the terahertz signals. In Fig. 11(b) the two THz-IR fields are applied between the states $|4\rangle \leftrightarrow (\frac{|a\rangle+|b\rangle}{2})$, $|6\rangle \leftrightarrow (\frac{|b\rangle+|c\rangle}{2})$ respectively.

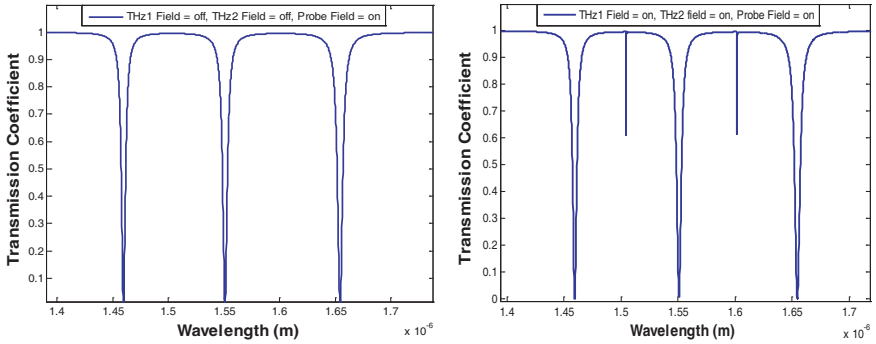

Figure 11. Transmission coefficient of probe field vs. wavelength. (a) For THz-IR fields is off. (b) For THz-IR fields is on.

Figure 12(a) shows another interesting case when the THz-IR fields are applied to states $|4\rangle \leftrightarrow |a\rangle$, $|4\rangle \leftrightarrow |b\rangle$, $|4\rangle \leftrightarrow |c\rangle$ or states $|6\rangle \leftrightarrow |a\rangle$, $|6\rangle \leftrightarrow |b\rangle$, $|6\rangle \leftrightarrow |c\rangle$. In the transmission coefficient of probe field we see transparency where there was absorption related to state $|1\rangle \leftrightarrow |a\rangle$, $|1\rangle \leftrightarrow |b\rangle$, $|1\rangle \leftrightarrow |c\rangle$. It is clear that the magnitude of these absorptions or transparencies (THz-IR field crated) is proportional to the THz-IR radiation intensities. Thermal energy that comes from environment temperature added to the THz-IR signal energy, so causes a detuning in fields. This detuning changes the absorption or transmission wavelength of probe field (wavelength shifting). There is an interesting case that is shown in Figs. 12(b) and (c), when the detuning of THz-IR signals are the same ($\Delta_{THz1} = \Delta_{THz2}$), wavelength shifting effect from thermal energy can be canceled. This is also due to the quantum well structure designation. The wavelength shifting of THz-IR signals are opposite because of the quantum well structure, so for a definite temperature (definite detuning) we can cancel this effect. This effect is so important from the photodetector point of view.

The parameters of the considered structures are given in Table 1 [12, 13, 20].

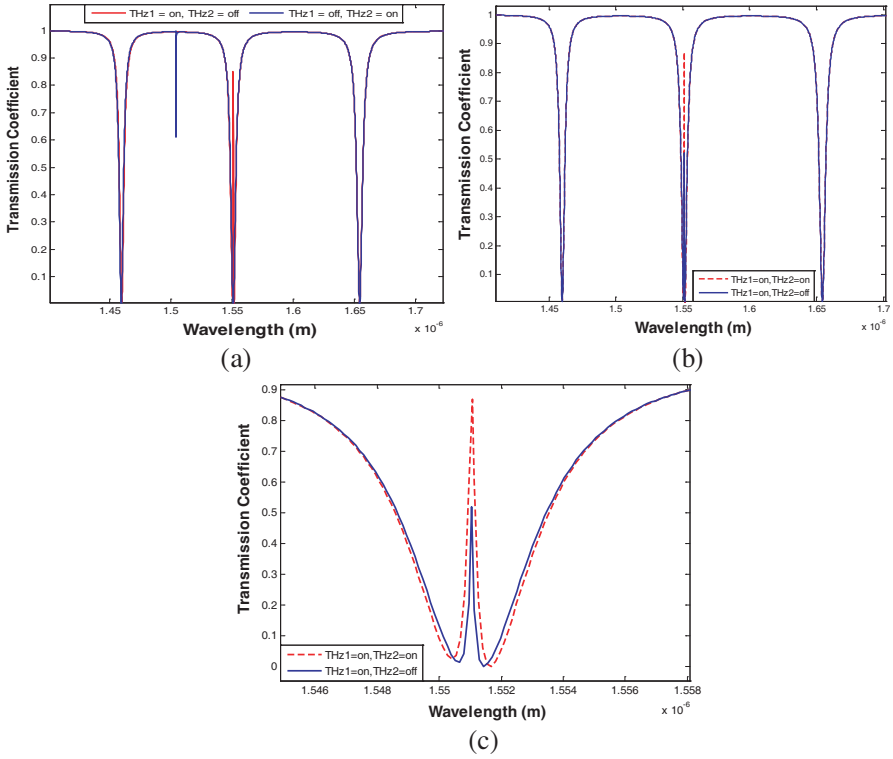

Figure 12. Transmission coefficient of probe field vs. wavelength. (a) In the presence of THz-IR fields. (b) and (c) The effect of temperature in the case when ($\Delta_{THz1} = \Delta_{THz2}$).

Table 1. Material parameters.

Atomic structure	Quantum well structure
$\Omega_c = 10^{12}\,\mathrm{s}^{-1},\ \Omega_p = 10^{8}\,\mathrm{s}^{-1},$ $\Omega_{IR} = 10^{10}\,\mathrm{s}^{-1} \sim 10^{11}\,\mathrm{s}^{-1}$ $N_a = 10^{181}/\mathrm{cm}^3,\ \gamma_{41} = 10^{11}\,\mathrm{s}^{-1},$ $\gamma_{21} = 10^{7}\,\mathrm{s}^{-1},\ \gamma_{31} = 10^{7}\,\mathrm{s}^{-1}$ $\gamma_{51} \cong \gamma_{61} = 10^{6}\,\mathrm{s}^{-1},$	$\Omega_{IR} = 10^{10} \sim 20^{11}\,\mathrm{s}^{-1},$ $\Omega_p = 10^{8}\,\mathrm{s}^{-1},\ E_s = 100\,\mathrm{meV}$ $N_a = 10^{17}\mathrm{cm}^{-3},$ $\Gamma_{ab} = \gamma_a + \gamma_{ab}^{dph} \approx 4.9\,\mathrm{meV},$ $q = \frac{\mu_{ab}}{\mu_{cb}}, K = \frac{\mu_{da}}{\mu_{dc}}$ $\Gamma_{cb} = \gamma_c + \gamma_{cb}^{dph} \approx 4.2\,\mathrm{meV},$ $\Gamma_{ac} = \gamma_a + \gamma_c + \gamma_{ac}^{dph} \approx 8.3\,\mathrm{meV}$

4. SUMMARY

In this paper, a novel room temperature Terahertz photodetector based on EIT in atomic structures and quantum well cascade structure has been presented. The results of simulations show that in the proposed structures the electromagnetic quantum interference between long wavelength and short-wavelength radiation modifies the absorption characteristic of short-wavelength probe field. By this means, the terahertz signal does not interact directly with ground state electrons, but affects on the absorption characteristics of the short-wavelength or visible probe optical field which directly interact with ground state electrons. Therefore, the important thermionic dark current in terahertz detection, can be strongly reduced in proposed 4-levels atomic and quantum well cascade structure and canceled out in proposed 6-levels atomic system and realized quantum well structure. Our proposed atomic structures can be realized with quantum well and quantum well cascade structures. It was shown that in the presence of THz-IR radiation, we see new absorption where there was transparency or the new transparence peak can be appeared in short wavelengths where there was a sharp absorption. The magnitude of these absorption or transparency peaks was related to the incoming THz-IR radiation intensity. So our proposed structures can be basic cell of room temperature Terahertz infrared photodetection.

REFERENCES

1. Diakides, N. A. and J. D. Bronzino, *Medical Infrared Imaging*, CRC Press, 2008.
2. Ganichev, S. D. and W. Prettl, *Intense Terahertz Excitation of Semiconductors*, Oxford University Press, 2006.
3. Miles, R. E., X. C. Zhang, H. Eisele, and A. Krotkus, *Terahertz Frequency Detection and Identification of Material and Object*, Springer, 2006.
4. Schneider, H. and H. C. Liu, *Quantum Well Infrared Photodetectors*, Springer, 2006.
5. Paiella, R., *Intersubband Transitions in Quantum Structures*, McGraw-Hill, 2006.
6. Levine, B. F., "Quantum well infrared photodetectors," *Appl. Phys.*, Vol. 74, R1–R81, 1993.
7. Etteh, N. E. I. and P. Harrison, "Carrier scattering approach to the origins of dark current in mid and far-infrared (terahertz)

quantum-well intersubband photodetectors (QWLPs)," *IEEE J. Quantum Electron.*, Vol. 37, 672–675, 2001.

8. Fleischhauer, M., A. Imamoglu, and J. P. Marangos, "Electromagnetically induced transparency: Optics in coherent media," *Rev. Mod. Phys.*, Vol. 77, 633–673, 2005.
9. Scully, M. O. and M. S. Zubairy, *Quantum Optics*, Cambridge University Press, 1997.
10. Zyaei, M., H. Rasooli Saghai, K. Abbasian, and A. Rostami, "Long wavelength infrared photodetector design based on electromagnetically induced transparency," *Optics Comm.*, Vol. 281, 3739–3747, 2008.
11. Rostami, A., M. Zyaei, H. Rasooli Saghai, and F. J. Sharifi, "Terahertz asymmetric quantum well infrared photodetector design based on electromagnetically induced transparency," *SPIE*, Vol. 7266, 72660Z-1, 2008.
12. Sandhya, N. and K. K. Sharma, "Atomic coherence effects in four-level systems: Doppler-free absorption within an electromagnetically-induced-transparency window," *Phys. Rev. A*, Vol. 55, 2155–2158, 1997.
13. Banacloche, J. G., Y. Q. Li, S. Z. Jin, and M. Xiao, "Electromagnetically induced transparency in ladder-type inhomogeneously broadened media: Theory and experiment," *Phys. Rev. A*, Vol. 51, 576–584, 1995.
14. Phillips, C. C., E. Paspalakis, G. B. Serapiglia, C. Sirtori, and K. L. Vodopyanov, "Observation of electromagnetically induced transparency and measurements of subband dynamics in a semiconductor quantum well," *Physica E*, Vol. 7, 166–173, 2000.
15. Dynes, J. F., M. D. Frogley, M. Beck, J. Faist, and C. C. Phillips, "Optically mediated coherent population trapping in asymmetric semiconductor quantum wells," *Phys. Rev. B*, Vol. 72, 085323–085329, 2005.
16. Wu, J. H., J. Y. Gao, J. H. Xu, L. silvestri, M. Artoni, G. C. La Rocca, and F. Bassani, "Ultrafast all optical switching via tunable fano interference," *Phys. Rev. Lett.*, Vol. 95, 057401–057406, 2005.
17. Schmidt, H. and A. Imamoglu, "Nonlinear optical devices based on a transparency in semiconductor intersubband transitions," *Opt. Comm.*, Vol. 131, 333–338, 1996.
18. Faist, J., F. Capasso, C. Sirtori, K. West, and L. N. Pfeiffer, "Controlling the sign of quantum interference by tunneling from quantum wells," *Nature*, Vol. 390, 589–591, 1997.
19. Sun, H., S. Gong, Y. Niu, S. Jin, R. Li, and Z. Xu, "Enhancing

Kerr nonlinearity in an asymmetric double quantum well via Fano interference," *Phys. Rev. B*, Vol. 74, 155314–155318, 2006.

20. Li, J.-H., "Controllable optical bistability in a four-subband semiconductor quantum well system," *Phys. Rev B*, Vol. 75, 155329–155334, 2007.